Prop-2-en-1-one Derivatives as Corrosion Inhibitors for Copper in 1 M HNO₃

A.S.Fouda[1,], A.M.Eldesoky[2], A.Z. El-Sonbati[3] and S.F.Salam[1]*

[1] Department of Chemistry, Faculty of Science, El-Mansoura University, El-Mansoura-35516, Egypt
[2] Engineering Chemistry Department, High Institute of Engineering &Technology (New Damietta), Egypt and Chemistry Department, Qunfudah University College, Umm Al-Qura University, KSA.
[3] Chemistry Department, Faculty of Science, Damietta University, Damietta, Egypt
[*]E-mail: asfouda@hotmail.com

Inhibition of corrosion of copper in nitric acid by prop-2-en-1-one derivatives has been studied using weight loss and electrochemical measurements. It was found that the prop-2-en-1-one derivatives act as a good corrosion inhibitor for copper in all concentrations of the prop-2-en-1-one derivatives. The inhibition action depends on the concentration of the prop-2-en-1-one derivatives in the acid solution. Results for weight loss and electrochemical measurements indicate that inhibition efficiency increases with increasing inhibitor concentration. Polarization curves revealed that these compounds are mixed type inhibitors. The adsorption of prop-2-en-1-one derivatives on the surface of the copper specimens obeys Temkin adsorption isotherm. Some thermodynamic and kinetic parameters for the corrosion process were estimated, and the values support the results obtained. Some quantum chemical parameters and the Mulliken charge densities for prop-2-en-1-one derivatives were calculated by the DFT (density function theory) semi-empirical method to provide further insight into the mechanism of inhibition of the corrosion process.

Keywords: prop-2-en-1-one derivatives, corrosion inhibition, copper, HNO₃, EFM, EIS

1. INTRODUCTION

Copper metallization has been used in integrated circuits for high-speed logic devices instead of the conventional aluminuim alloy metallization because of its excellent electrical and thermal conductivity [1-3]. However, it is well known that copper is very susceptible to corrosion in aqueous media and the corrosion products cause a decrease in the electrical conductivity of the devices [4,5]. Thus, much attention has been focused on the behavior of various inhibitors in different media to find the conditions for preventing copper corrosion. Many investigators [6-9] have studied to obtain optimum corrosion protection for copper in various aqueous solutions by either finding new inhibitors

or improving the inhibition efficiency [10]. Most acid corrosion inhibitors are nitrogen, sulfur, or oxygen containing organic compounds. Among these compounds it is generally known that heterocyclic compounds, especially N-based ones, are effective inhibitors for copper corrosion in aqueous solutions [11]. Especially, imidazole and its derivatives are of interest as corrosion inhibitors for copper metal and alloys [12-15]. Imidazole is a planar, aromatic heterocyclic organic compound with two N atoms forming part of a five membered ring [16]. One of the N atoms is of the pyrrole type and the other is a pyridine-like one. Despite extensive studies undertaken on imidazole, until now, it is still questionable what mechanism is adequate for the explanation of the inhibition of copper corrosion by imidazole in acid solutions.

The objective of this work is to identify four selected prop-2-en-1-one derivatives as corrosion inhibitors for copper in 1 M HNO_3 by different methods and to analyze the surface morphology of inhibited copper by scanning electron microscope technology with energy dispersive X-ray spectroscopy (SEM–EDX).

2. EXPERIMENTAL DETAIL

2.1. Composition of material samples

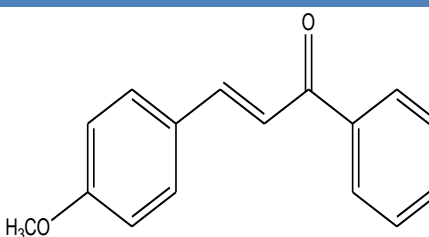**Table 1.** Chemical composition of the copper used in this investigation in weight % is as follows

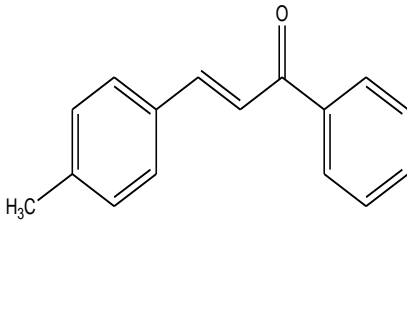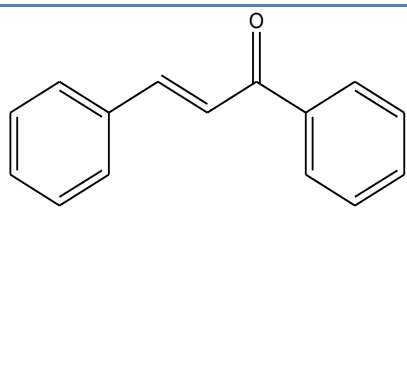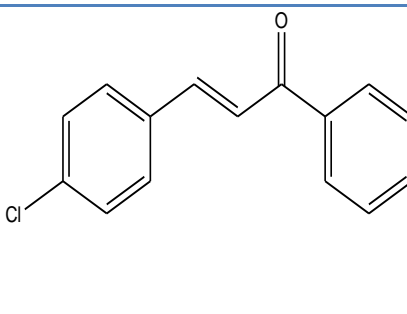| Element	Sn	Ag	Fe	Zn	Pb	As	Cu
Weight %	0.001	0.001	0.01	0.05	0.002	0.0002	The rest

2.2. Chemicals and solutions

Nitric acid (BDH grade) and organic additives (inhibitors)

The organic inhibitors used in this study were synthesized in the laboratory as before [17], and are listed in Table (2):

Table 2. Chemical structures, names, molecular weights and molecular formulas of prop-2-en-1-one derivatives

Comp	Structure	Name	Mol. Weights / Mol.Formula
1		(E)-3-(4-methoxy phenyl)-1-phenyl prop-2-en-1-one	$C_{16}H_{14}O_2$ 238.29

2		(E)-3-(4-methylphenyl)-1-phenyl prop-2-en-1-one	$C_{16}H_{14}O$ 222.29
3		(E)-3-(phenyl)-1-phenyl prop-2-en-1-one	$C_{15}H_{12}O$ 208.26
4		(E)-3-(4-choloro phenyl)-1-phenyl prop-2-en-1-one	$C_{15}H_{11Cl}$ 242.7

2.3 Methods used for corrosion measurements

2.3.1 Weight loss tests

For weight loss measurements, square specimens of size 2 x 2 x 0.2 cm were used. The specimens were first polished to a mirror finish using 400 up to 1200 grit emery paper, degreased in methanol and finally washed with bidistilled water and dried before being weighed. The specimens then immersed into 100 ml of the test solution. The weight loss measurements were carried out in a 100 ml capacity glass beaker placed in water thermostat. The specimens were then immediately immersed in the test solution without or with desired concentration of the investigated compounds. Triplicate specimens were exposed for each condition and the mean weight losses were reported in order to verify reproducibility of the experiments.

2.3.2 Potentiodynamic polarization measurements

Polarization experiments were carried out in a conventional three-electrode cell with platinum gauze as the auxiliary electrode and a saturated calomel electrode (SCE) coupled to a fine Luggin

capillary as reference electrode. The working electrode was in the form of a square cut from copper sheet of equal composition embedded in epoxy resin of polytetrafluoroethylene so that the flat surface area was 1 cm^2. Prior to each measurement, the electrode surface was pretreated in the same manner as the weight loss experiments. Before measurements, the electrode was immersed in solution at natural potential for 30 min until a steady state was reached. The potential was started from - 600 to + 400 mV vs open circuit potential (E_{ocp}). All experiments were carried out in freshly prepared solutions at 30°C and results were always repeated at least three times to check the reproducibility.

2.3.3 Electrochemical impedance spectroscopy measurements

Impedance measurements were carried out using AC signals of 5 mV peak to peak amplitude at the open circuit potential in the frequency range of 100 kHz to 0.1 Hz. All impedance data were fitted to appropriate equivalent circuit using the Gamry Echem Analyst software.

2.3.4 Electrochemical frequency modulation measurements

EFM experiments were performed with applying potential perturbation signal with amplitude 10 mV with two sine waves of 2 and 5 Hz. The choice for the frequencies of 2 and 5 Hz was based on three arguments [18]. The larger peaks were used to calculate the corrosion current density (i_{corr}), the Tafel slopes (β_c and β_a) and the causality factors CF-2 and CF-3 [19].

All electrochemical experiments were carried out using Gamry instrument PCI300/4 Potentiostat/Galvanostat/Zra analyzer, DC 105 corrosion software, EIS 300 electrochemical impedance spectroscopy software, EFM 140 electrochemical frequency modulation software and Echem Analyst 5.5 for results plotting, graphing, data fitting and calculating.

2.3.5 SEM-EDX measurements

The copper surface was prepared by keeping the specimens for 3 days in 1 M HNO_3 in the presence and absence of optimum concentration of investigated organic derivatives, after abraded using different emery papers up to 1200 grit size and then polished with Al_2O_3 (0.5 m particles size), after this immersion time, the specimens were washed gently with bidistilled water, carefully dried and mounted into the spectrometer without any further treatment. The corroded copper surfaces were examined using an X-ray diffractometer Philips (pw-1390) with Cu-tube (Cu Ka1, l = 1.54051 A°), a scanning electron microscope (SEM, JOEL, JSM-T20, Japan).

2.3.6 Theoretical study

Accelrys (Material Studio Version 4.4) software for quantum chemical calculations has been used.

3. RESULTS AND DISCUSSION

3.1. Weight loss measurements

Figure (1) represents the weight loss-time curves for copper in 1 M HNO_3 in the absence and presence of different concentrations of compound (1). Similar curves were obtained for other inhibitors (not shown). Table (3) collects the values of inhibition efficiency obtained from weight loss measurements in 1 M HNO_3 at 30 ± 0.1 °C. The results of this Table show that the presence of inhibitors reduces the corrosion rate of copper in 1 M HNO_3 and hence, increase the inhibition efficiency. The inhibition achieved by these compounds decreases in the following order: Compound (1) > Compound (2) > Compound (3) > Compound (4)
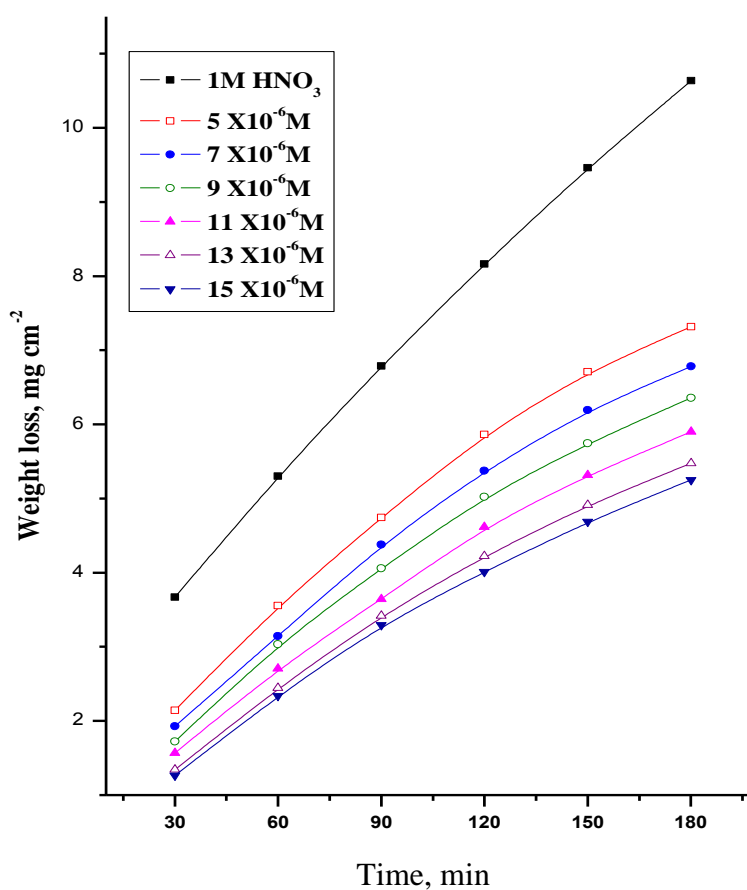

Figure 1. Weight loss-time curves for copper dissolution in 1M HNO_3 in absence and presence of different concentrations of inhibitor (1) at 30 °C

Table 3. Data of weight loss measurements for copper in 1 M HNO_3 solution in the absence and presence of different concentrations of investigated compounds at 30 °C

Conc., M	%IE			
	(1)	(2)	(3)	(4)
5×10^{-6}	67.3	62.1	57.4	43.0
7×10^{-6}	70.4	64.3	58.0	45.7

9×10^{-6}	73.0	67.9	64.1	50.3
11×10^{-6}	75.9	72.8	64.2	53.8
13×10^{-6}	77.1	73.1	68.6	53.9
15×10^{-6}	80.2	75.0	70.8	58.3

3.2. Adsorption isotherm

It is widely acknowledge that adsorption isotherm provide useful insight onto the mechanism of corrosion inhibition as well as the interaction among the adsorbed molecules themselves and their interaction with the electrode surface [20]. In this study, Temkin adsorption isotherm was found to be suitable for the experimental results. The isotherm is described by the following equation:

$\theta = 2.303/a \log K_{ads} + 2.303/a \log C$ (1)

where C is the inhibitor concentration, K_{ads} is the adsorption equilibrium constant. The plot of θ versus log C gives linear relation (shown in Figure 2). The adsorption equilibrium constant K_{ads} can be calculated from the intercept and ΔG^{o}_{ads} can be calculated from the following equation:

$\log K_{ads} = -\log 55.5 - \Delta G^{o}_{ads} / 2.303RT$ (2)

where value of 55.5 is the concentration of water in solution in mole/liter [21], R is the universal gas constant and T is the absolute temperature. It was noticed that the value of ΔG^{o}_{ads} has a negative sign ensure the spontaneity of the adsorption and stability of the adsorbed layer on the alloy surface [22] [Table 4]. Also the values of ΔG^{o}_{ads} are around 40 kJ mol^{-1} which was attributed to electrostatic interactions between inhibitors species and the charged metal surface (physisorption). The values of K_{ads} were found to run parallel to the % IE [K (1) > K (2) > K (3) > K (4)] [Table 4].This result reflects the increasing capability, due to structural formation, on the metal surface [23].
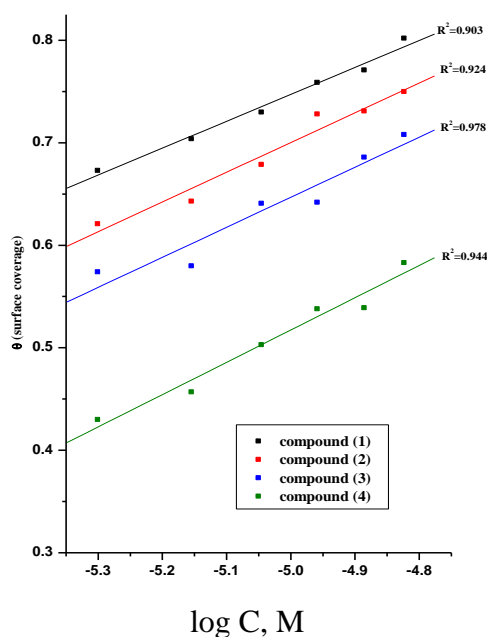

Figure 2. Curve fitting of corrosion data for copper in 1 M HNO$_3$ in presence of different concentrations of inhibitors to the Temkin isotherm at 30°C

Table 4. Inhibitor binding constant (K_{ads}), free energy of binding ($\Delta G°_{ads.}$) and later interaction parameter (a) for inhibitors at 30°C

Inhibitors	Temkin		
	a	K_{ads}	$-\Delta G°_{ads.,}$ kJ mol^{-1}
Compound (1)	13.03	69.2	63.9
Compound (2)	12.30	60.4	62.6
Compound (3)	13.08	26.0	53.1
Compound (4)	13.43	20.23	38.7

3.3. Effect of Temperature

The effect of temperature on the inhibited acid-metal reaction is highly complex, because many changes occur on the metal surface, such as rapid etching and desorption of the inhibitor and the inhibitor itself, in some cases, may undergo decomposition and/or rearrangement. Generally the corrosion rate increases with the rise of temperature. It was found that the inhibition efficiency decreases with increasing temperature and increases with increasing the concentration of the inhibitor. The activation energy (E^*_a) of the corrosion process was calculated using Arrhenius equation [24]:

$$C.R. = A \exp(-E^*_a / RT) \qquad (3)$$

where C.R. corrosion rate and A is Arrhenius constant The values of activation energies E^*_a can be obtained from the slope of the straight lines of plotting log C.R. vs. 1/T in the presence and absence of investigated compounds at various temperatures as shown in Figure (3) and in Table (5). It is noted that the values of activation energy increase in the presence of inhibitors and with increase of the concentration of the inhibitors. This is due to the formation of a film of inhibitors on copper surface. The activation energy for the corrosion of copper in 1 M HNO_3 was found to be 51.9 kJ mol^{-1} which is in good agreement with the work carried out by Fouda et al [25] and others [26-27] An alternative formulation of the Arrhenius equation is the transition state equation 4 [28]:

$$C.R. = RT/Nh \exp(\Delta S^*/R) \exp(-\Delta H^*/RT) \qquad (4)$$

where h is Planck's constant, N is Avogadro's number, ΔS^* is the entropy of activation and ΔH^* is the enthalpy of activation. Figure (4) shows a plot of log (C.R. / T) vs. (1/T). Straight lines are obtained with a slope of ($\Delta H^*/2.303 R$) and an intercept of (log R/Nh + $\Delta S^*/2.303 R$) from which the values of ΔH^* and ΔS^* are calculated and also listed in Table (4). From inspection of Table (5) it is clear that the positive values of ΔH^* reflect that the process of adsorption of the inhibitors on the copper surface is an endothermic process; it is attributable unequivocally to chemisorption [29]. Typically, the enthalpy of a chemisorption process approaches 100 kJ mol^{-1} .More interesting behavior was observed in Table (5) that positive ΔS^* values is accompanied with endothermic adsorption process. This is agrees with what expected, when the adsorption is an endothermic process, it must be accompanied by an increase in the entropy change and vies versa [30].

It is seen that investigated derivatives have inhibiting properties at all the studied temperatures and the values of % IE decrease with temperature increase. This shows that the inhibitor has experienced a significant decrease in its protective properties with increase in temperature. This

decrease in the protective properties of the inhibitor with increase in temperature may be connected with two effects; a certain drawing of the adsorption-desorption equilibrium towards desorption (meaning that the strength of adsorption process decreases at higher temperatures) and roughening of the metal surface which results from enhanced corrosion. These results suggest that physical adsorption may be the type of adsorption of the inhibitor on the copper surface.
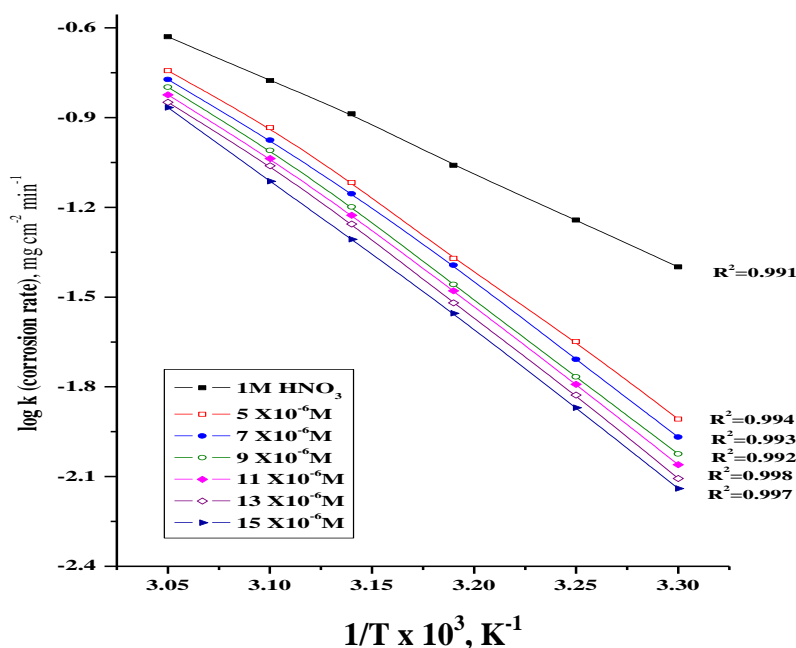

Figure 3. log k (corrosion rate) - 1/T curves for copper dissolution in 1M HNO₃ in absence and presence of different concentrations of inhibitor (1)

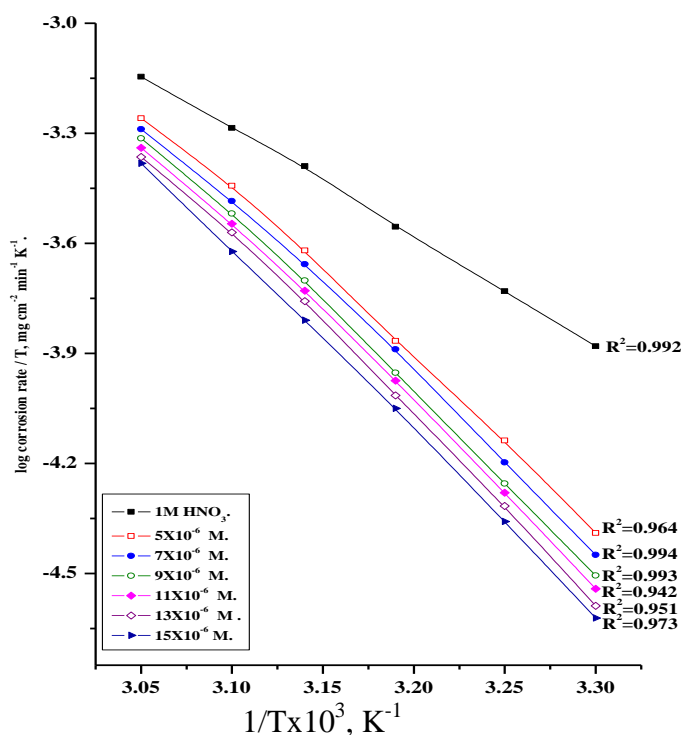**Figure 4.** log (corrosion rate/T) - (1/T) curves for copper dissolution in 1M HNO₃ in absence and presence of different concentrations of inhibitor (1)

Table 5. Activation parameters for the dissolution of copper in the presence and absence of different
concentrations of inhibitors in 1M HNO_3

Inhibitor	Conc., M.	Activation parameters		
		E_a^*	ΔH^*	ΔS^*
		$kJ\ mol^{-1}$	$kJ\ mol^{-1}$	$J\ mol^{-1}\ K^{-1}$
Free Acid 1M HNO_3	0.0	51.9	51.2	81.3
Compound (1)	5×10^{-6}	84.9	86.2	16.4
	7×10^{-6}	93.6	89.4	12.2
	9×10^{-6}	94.9	91.3	10.6
	11×10^{-6}	95.3	90.7	10.2
	13×10^{-6}	95.9	92.8	5. 7
	15×10^{-6}	96.9	94.1	5. 4
Compound (2)	5×10^{-6}	78.9	76.5	25.1
	7×10^{-6}	80.2	78.5	19.3
	9×10^{-6}	83.1	80.4	14.2
	11×10^{-6}	83.9	81.2	12.4
	13×10^{-6}	83.7	81.2	8.6
	15×10^{-6}	85.0	83.2	7.6
Compound (3)	5×10^{-6}	67.3	71.2	41.0
	7×10^{-6}	74.0	71.7	36.4
	9×10^{-6}	74.9	74.0	33.4
	11×10^{-6}	76.8	75.4	28.5
	13×10^{-6}	77.9	79.3	17.3
	15×10^{-6}	80.2	80.2	13.3
Compound (4)	5×10^{-6}	61.4	67.0	54.2
	7×10^{-6}	70.2	67.1	53.3
	9×10^{-6}	70.2	68.2	51.6
	11×10^{-6}	71.9	69.0	47.8
	13×10^{-6}	72.8	69.8	47.3
	15×10^{-6}	72.9	70.1	46.2

3.4. Potentiodynamic polarization measurements

Theoretically, copper can hardly be corroded in the deoxygenated acid solutions, as copper cannot displace hydrogen from acid solutions according to the theories of chemical thermodynamics [31-33]. However, this situation will change in nitric acid. Dissolved oxygen may be reduced on copper surface and this will allow corrosion to occur. It is a good approximation to ignore the hydrogen evolution reaction and only consider oxygen reduction in the nitric acid solutions at potentials near the corrosion potentials [34]. Polarization measurements were carried out in order to gain knowledge concerning the kinetics of the cathodic and anodic reactions. Figure (5) shows the polarization behavior of copper electrode in 1 M HNO_3 in the absence and presence of various concentrations of compound (1). Figure (5) shows that both the anodic and cathodic reactions are affected by the addition of investigated organic derivatives and the inhibition efficiency increases as

the inhibitor concentration increases, but the cathodic reaction is more inhibited, meaning that the addition of inhibitors reduces the anodic dissolution of copper and also retards the cathodic reactions. Therefore, investigated derivatives are considered as mixed type inhibitors. The values of electrochemical parameters such as corrosion current densities (i_{corr}), corrosion potential (E_{corr}), the cathodic Tafel slope (β_c), anodic Tafel slope (β_a) and inhibition efficiency (% IE) were calculated from the curves of Fig. 5 and are listed in Table (6).
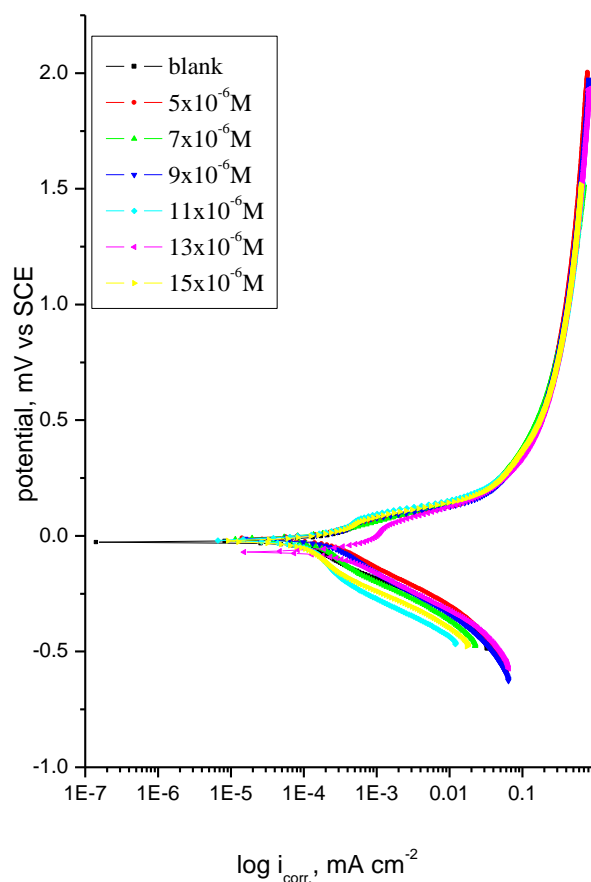

Figure 5. Potentiodynamic polarization curves for the corrosion of copper in 1 M HNO_3 in the absence and presence of various concentrations of compound (1) at 30°C

The results in Table (6) revealed that the corrosion current density decreases obviously after the addition of inhibitors in 1 M HNO_3 and % IE increases with increasing the inhibitor concentration. In the presence of inhibitors E_{corr} was enhanced with no definite trend, indicating that these compounds act as mixed–type inhibitors in 1 M HNO_3. The inhibition efficiency and the degree of surface coverage (θ) were calculated using equation 5:

$$\% \ IE_p = \theta \times 100 = [(i^o_{corr} - i_{corr}) / i^o_{corr}] \times 100 \qquad (5)$$

where i^o_{corr} and i_{corr} are the uninhibited and inhibited corrosion current densities, respectively.

Also it is obvious from Table (6) that the slopes of the anodic (β_a) and cathodic (β_c) Tafel lines remain almost unchanged upon addition of tested derivatives, giving rise to a nearly parallel set of anodic lines, and almost parallel cathodic plots results too. Thus the adsorbed inhibitors act by simple

blocking of the active sites for both anodic and cathodic processes. In other words, the adsorbed inhibitors decrease the surface area for corrosion without affecting the corrosion mechanism of copper in 1 M HNO$_3$ solution, and only causes inactivation of a part of the surface with respect to the corrosive medium [35,36]. The inhibition efficiency of these compounds follows the sequence: compound (1) > compound (2) >compound (3) > compound (4).

This sequence may attribute to free electron pair in oxygen atom, π electrons on aromatic nuclei and the substituent in the molecular structure of the inhibitor, and again reflects, as confirmed from weight loss measurements, the increased ability of compound (1) to inhibit nitric acid corrosion of copper as compared to compound (4). This is clearly seen from the highest efficiency recorded for compound (1).

Table 6. Effect of concentrations of the investigated compounds (1- 4) on the free corrosion potential (E$_{corr.}$), corrosion current density (i$_{corr.}$), Tafel slopes (β_a & β_c), degree of surface coverage (θ) and inhibition efficiency (% IE) for copper in 1M HNO$_3$ at 30°C

Concentration, M	i$_{corr.}$ mA cm^{-2}	-E$_{corr.}$ mV vs. SCE	β_a mV dec^{-1}	β_c mV dec^{-1}	θ	% IE
1M HNO$_3$	9.60	268	82	167	-	-
(1) 5 x 10^{-6}	1.3	261	90	339	86.5	86.5
7 x 10^{-6}	1.28	231	128	476.5	86.7	86.7
9 x 10^{-6}	1.2	255	96	266.2	87.5	87.5
11 x 10^{-6}	1.1	246	103	346.6	88.5	88.5
13 x 10^{-6}	1.07	268	95	175.3	88.9	88.9
15x 10^{-6}	1.03	203	81	129.4	89.3	89.3
(2) 5 x 10^{-6}	1.77	209	93	163.4	81.6	81.6
7 x 10^{-6}	1.61	221	84	282.9	83.2	83.2
9 x 10^{-6}	1.66	240	52	99.7	82.7	82.7
11 x 10^{-6}	1.55	278	99	65.1	83.9	83.9
13 x 10^{-6}	1.4	691	44	72.9	85.4	85.4
15x 10^{-6}	1.37	233	111	342.6	85.7	85.7
(3) 5 x 10^{-6}	3.9	638	95.5	192	59.4	59.4
7 x 10^{-6}	3.89	263	129.2	313.3	59.5	59.5
9 x 10^{-6}	3.27	367	117.4	197.7	65.9	65.9
11 x 10^{-6}	3.21	566	65.3	100	66.5	66.56
13 x 10^{-6}	2.3	648	100.9	209.3	76	76.04
15x 10^{-6}	2.21	952	110.8	184.2	76.9	76.97
(4) 5 x 10^{-6}	4.97	287	148.8	246.8	0.482	48.2
7 x 10^{-6}	4.48	235	152.9	226.6	0.533	53.3
9 x 10^{-6}	4.33	222	96.0	174.9	0.548	54.8
11 x 10^{-6}	4.27	319	109.8	267.1	0.555	55.5
13 x 10^{-6}	4.11	427	100.4	208.0	0.571	57.1
15x 10^{-6}	4.01	512	53.5	150.2	0.582	58.2

3.5 Electrochemical impedance spectroscopy (EIS)

EIS is well-established and powerful technique in the study of corrosion. Surface properties, electrode kinetics and mechanistic information can be obtained from impedance diagrams [37-41]. Figure (6) shows the Nyquist (a) and Bode (b) plots obtained at open-circuit potential both in the absence and presence of increasing concentrations of investigated compounds at 30°C. The increase in the size of the capacitive loop with the addition of organic derivatives shows that a barrier gradually forms on the copper surface. The increase in the capacitive loop size (Figure 6a) enhances, at a fixed inhibitor concentration, following the order: compound (1) > compound (2) compound (3) > compound (4), confirming the highest inhibitive influence of compound (1). Bode plots (Figure 6b), shows that the total impedance increases with increasing inhibitor concentration (log Z vs. log f). But (log f vs. phase), also Bode plot shows the continuous increase in the phase angle shift, obviously correlating with the increase of inhibitor adsorbed on copper surface. The Nyquist plots do not yield perfect semicircles as expected from the theory of EIS. The deviation from ideal semicircle was generally attributed to the frequency dispersion [42] as well as to the inhomogeneities of the surface. EIS spectra of the tested additives were analyzed using the equivalent circuit, Figure (7), which represents a single charge transfer reaction and fits well with our experimental results. The constant phase element, CPE, is introduced in the circuit instead of a pure double layer capacitor to give a more accurate fit [43].The double layer capacitance, C_{dl}, for a circuit including a

$$C_{dl} = Y_0 \, \omega^{n-1} / \sin [n \, (\pi/2)] \qquad (6)$$

where Y_0 is the magnitude of the CPE, $\omega = 2\pi f_{max}$, f_{max} is the frequency at which the imaginary component of the impedance is maximal and the factor n is an adjustable parameter that usually lies between 0.5 and 1.0. After analyzing the shape of the Nyquist plots, it is concluded that the curves approximated by a single capacitive semicircles, showing that the corrosion process was mainly charged-transfer controlled [45, 46]. The general shape of the curves is very similar for all samples (in presence or absence of inhibitors at different immersion times) indicating that no change in the corrosion mechanism [47]. From the impedance data (Table 7), we conclude that the value of R_{ct} increases with increasing the concentration of the inhibitors and this indicates an increase in % IE, which in concord with the weight loss results obtained. In fact the presence of inhibitors enhances the value of R_{ct} in acidic solution. Values of double layer capacitance are also brought down to the maximum extent in the presence of inhibitor and the decrease in the values of CPE follows the order similar to that obtained for i_{corr} in this study. The decrease in CPE/C_{dl} results from a decrease in local dielectric constant and/or an increase in the thickness of the double layer, suggesting that organic derivatives inhibit the iron corrosion by adsorption at metal/acid [48, 49]. The inhibition efficiency was calculated from the charge transfer resistance data from equation 7 [50]:

$$\% \, IE_{EIS} = [1 - (R^{\circ}_{ct} / R_{ct})] \times 100 \qquad (7)$$

where R^{o}_{ct} and R_{ct} are the charge-transfer resistance values without and with inhibitor respectively.
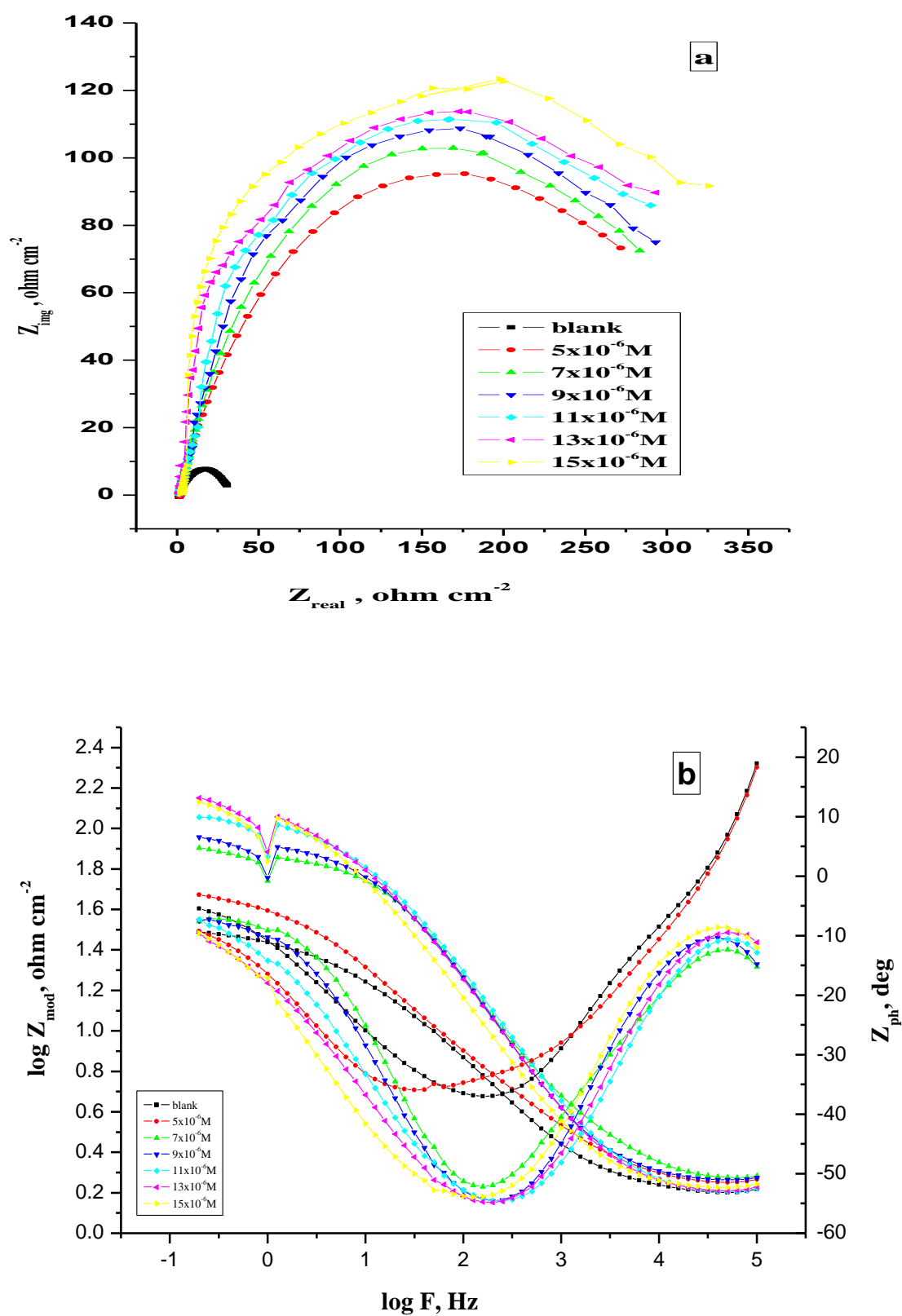
Figure 6. The Nyquist (a) and Bode (b) plots for corrosion of copper in 1 M HNO₃ in absence and presence of different concentrations of compound (1) at 30°C

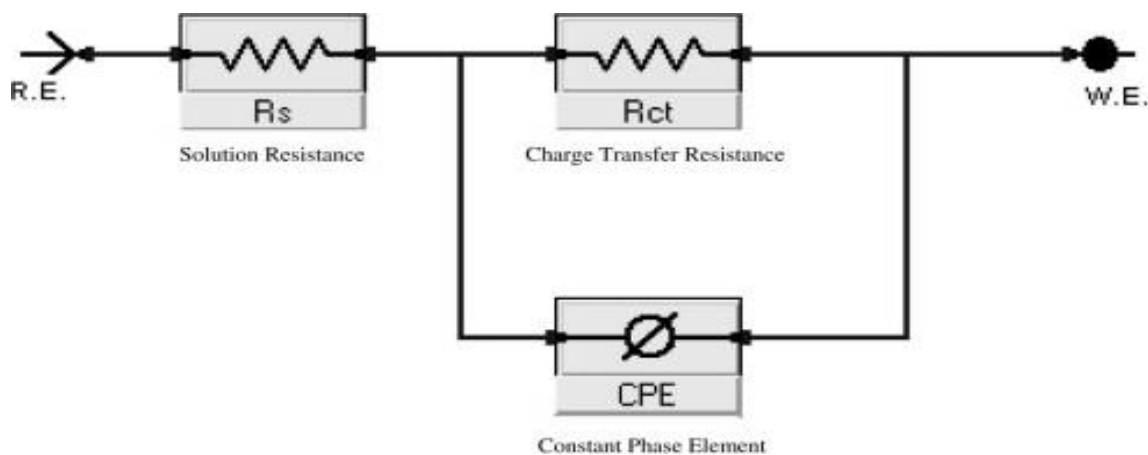**Figure 7.** Equivalent circuit model used to fit experimental EIS

Table 7. Electrochemical kinetic parameters obtained by EIS technique for copper in 1 M HNO_3 without and with various concentrations of compounds (1- 4) at 30°C

| Comp.	Conc., M	R_S, Ω cm^2	Y, x 10^{-3} $\mu\Omega^{-1}$ s^n	n	R_{CT}, Ω cm^2	C_{dl}, $\mu F cm^{-2}$	θ	%IE
	Blank	1.501	2.602	624.2	29.76	14.24	------	--------
(1)	5x10^{-6}	1.790	534.0	742.6	289.1	46964.4	0.897	89.7
	7x10^{-6}	1.855	652.3	726.7	300	85582.7	0.900	90.0
	9x10^{-6}	1.645	559.2	707.2	303.5	22313.08	0.901	90.1
	11x10^{-6}	1.66	707.8	713.8	307.7	31048.54	0.903	90.3
	13x10^{-6}	1.627	705.4	676.1	319.1	26205.81	0.906	90.6
	15x10^{-6}	1.877	568.4	709.0	346.5	95934.2	0.914	91.4
(2)	5x10^{-6}	1.887	954.4	679.5	200.5	10151.25	0.851	85.1
	7x10^{-6}	1.599	827.4	734.4	203.9	20001.21	85.4	85.4
	9x10^{-6}	1.601	830.7	717.7	213.2	20847.08	0.860	86.0
	11x10^{-6}	1.661	396.9	746.2	235.2	14662.27	0.873	87.3
	13x10^{-6}	1.559	466.1	748.9	285	10389.02	0.884	88.4
	15x10^{-6}	1.808	544.9	720.8	284.1	525326.4	0.895	89.5
(3)	5x10^{-6}	1.629	847.6	699.0	141.3	19082.28	0.800	80.0
	7x10^{-6}	1.626	985	687.3	148.9	22577.11	0.810	81.0
	9x10^{-6}	1.884	926.1	746.6	157.2	81060.62	0.825	825
	11x10^{-6}	1.956	1011	659.9	170.2	137.2614	0.833	83.3
	13x10^{-6}	1.878	553.4	724.3	178.9	52581.27	0.838	83.8
	15x10^{-6}	1.725	752.6	700.9	184.3	33042.29	0.789	78.9
(4)	5x10^{-6}	1,650	3.601	564.9	52.57	47.30	0.433	43.3
	7x10^{-6}	1.774	5.028	714.2	75.31	142.58	0.604	60.4
	9x10^{-6}	1.720	413.9	752.8	81.24	9813.521	0.633	63.36
	11x10^{-6}	1.450	488.9	718.7	108.4	4027.016	0.725	72.5
	13x10^{-6}	1.457	601.3	706.9	125.7	5476.303	0.763	76.3
	15x10^{-6}	1.535	764.6	704.8	127.0	10208.67	0.789	78.9

*3.6. Electrochemical Frequency Modulation Technique (EFM)*

EFM is a nondestructive corrosion measurement technique that can directly and quickly determine the corrosion current values without prior knowledge of Tafel slopes, and with only a small polarizing signal. These advantages of EFM technique make it an ideal candidate for online corrosion monitoring [51]. The great strength of the EFM is the causality factors which serve as an internal check on the validity of EFM measurement. The causality factors CF-2 and CF-3 are calculated from the frequency spectrum of the current responses.

Figure (8) shows the EFM Intermodulation spectrums of copper in nitric acid solution containing different concentrations of compound (1). Similar curves were obtained for other compounds (not shown). The harmonic and intermodulation peaks are clearly visible and are much larger than the background noise. The two large peaks, with amplitude of about 200 µA, are the response to the 40 and 100 mHz (2 and 5 Hz) excitation frequencies. It is important to note that between the peaks there is nearly no current response (<100 nA). The experimental EFM data were treated using two different models: complete diffusion control of the cathodic reaction and the "activation" model. For the latter, a set of three non-linear equations had been solved, assuming that the corrosion potential does not change due to the polarization of the working electrode [52]. The larger peaks were used to calculate the corrosion current density (i_{corr}), the Tafel slopes (β_c and β_a) and the causality factors (CF-2 and CF-3).These electrochemical parameters were listed in Table (8). The data presented in Table (8) obviously show that, the addition of any one of tested compounds at a given concentration to the acidic solution decreases the corrosion current density, indicating that these compounds inhibit the corrosion of copper in 1 M HNO_3 through adsorption. The causality factors obtained under different experimental conditions are approximately equal to the theoretical values (2 and 3) indicating that the measured data are verified and of good quality. The inhibition efficiencies % IE_{EFM} increase by increasing the inhibitor concentrations and was calculated as from equation 8:

$$\% \ IE_{EFM} = [1-(i_{corr}/ \ i^o_{corr})] \ x \ 100 \qquad (8)$$

where i^o_{corr} and i_{corr} are corrosion current densities in the absence and presence of inhibitor, respectively. The inhibition sufficiency obtained from this method is in the order: compound (1) > compound (2) compound (3) > compound (4)
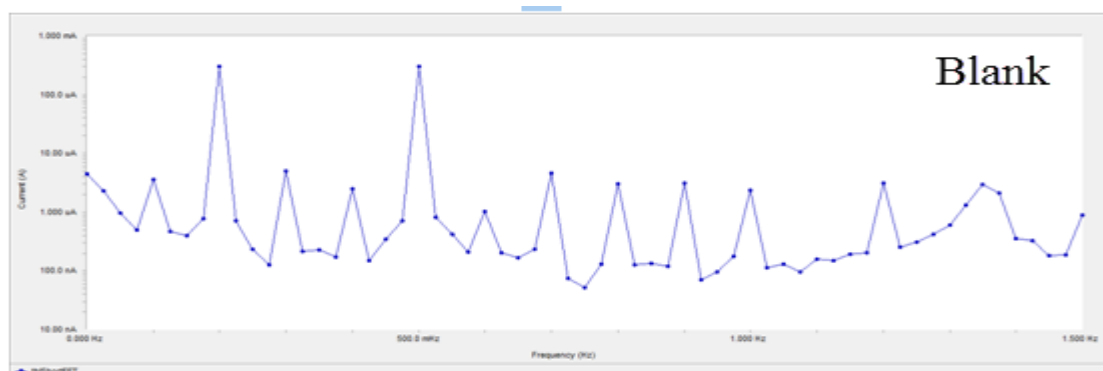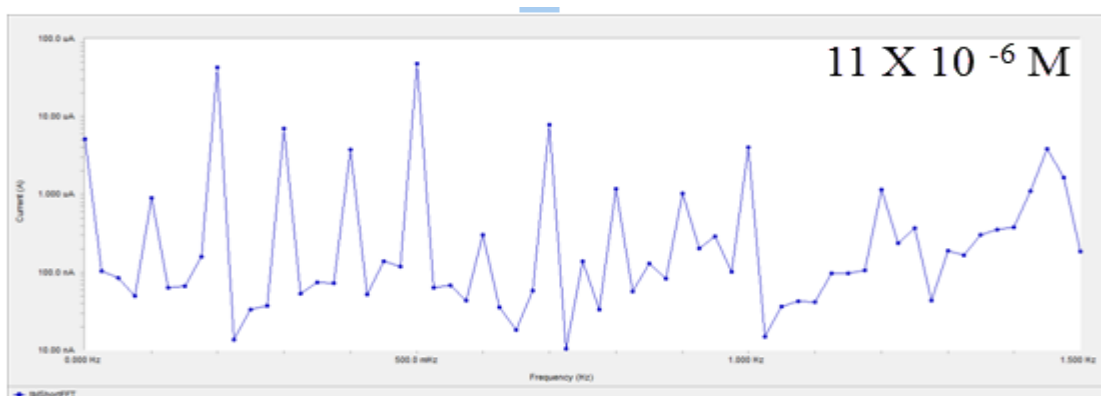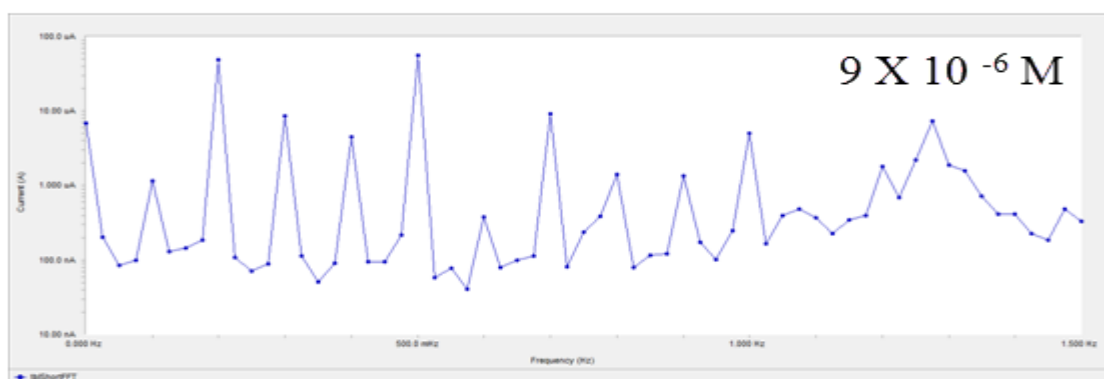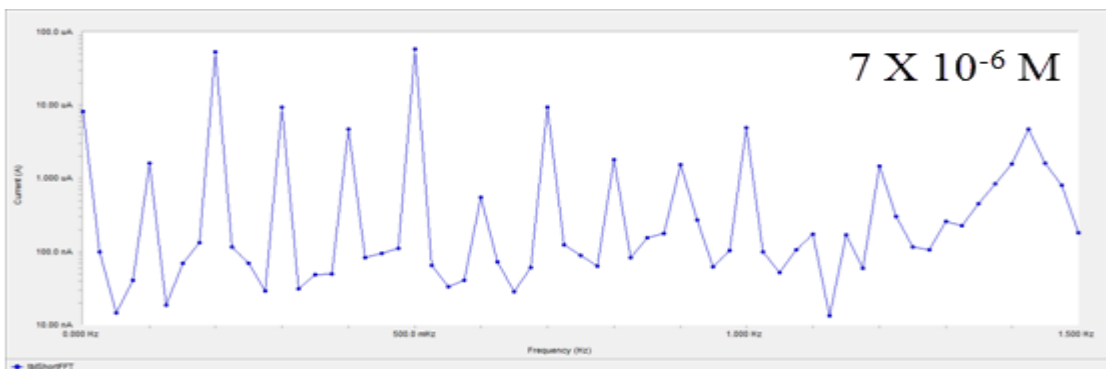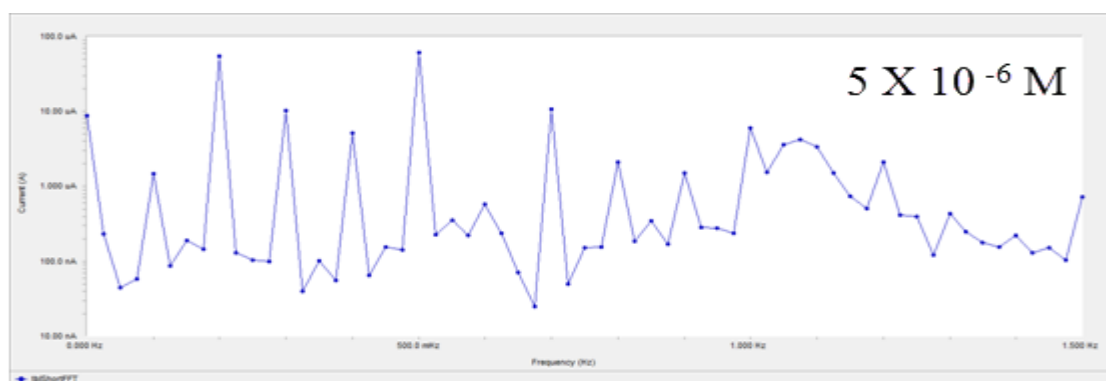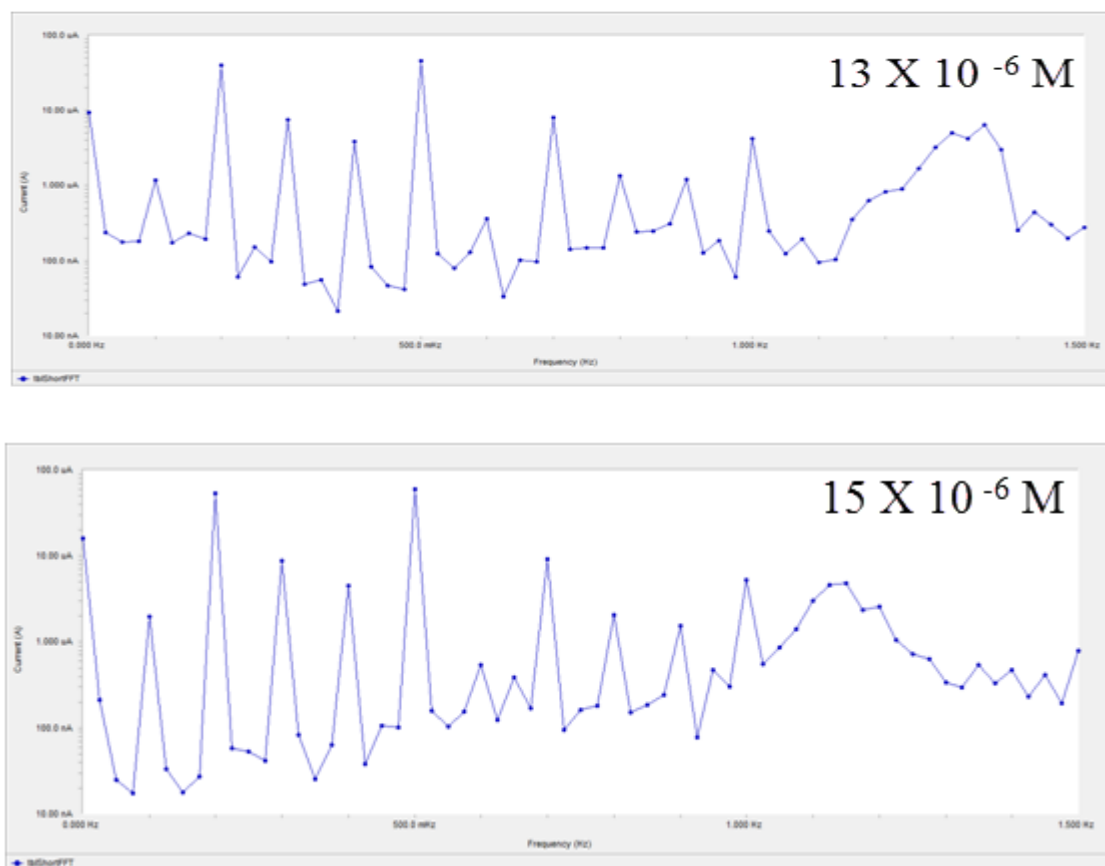
Figure 8. EFM spectra for copper in 1 M HNO₃ in the abscence and presence of different concentrations of compound (1)

Table 8. Electrochemical kinetic parameters obtained by EFM technique for copper in 1 M HNO3 without and with various concentrations of compounds (1 - 4) at 30°C

Comp.	Conc., M. M	i_{corr}, $\mu A\ cm^2$	β_a mV dec^{-1}	β_c mV dec^{-1}	CF-2	CF-3	% IE
Compound (1)	Blank	514	105.8	110	1.96	3.03	------
	5x10⁻⁶	75.41	57.49	159.7	1.87	2.79	85.32
	7x10⁻⁶	73.42	59.3	151.7	1.94	2.89	85.71
	9x10⁻⁶	72.35	61.21	169.5	1.85	3.07	85.92
	11x10⁻⁶	69.33	66.16	195.1	1.92	2.94	86.51
	13x10⁻⁶	63.51	62.79	207.9	1.95	3.09	87.64
	15x10⁻⁶	60.97	52.38	108	1.84	3.03	88.13
Compound (2)	5x10⁻⁶	102.2	54.55	133.2	1.96	3.09	80.11
	7x10⁻⁶	90.92	53.93	122.4	1.92	3.06	82.31
	9x10⁻⁶	84.99	63.13	223.6	1.87	3.03	83.46
	11x10⁻⁶	82.68	57.91	137.3	1.9	3.07	83.91
	13x10⁻⁶	81.63	56.21	168	1.97	3.02	84.11
	15x10⁻⁶	75.52	59.57	186.6	1.95	3.06	85.3
Compound (3)	5x10-6	182.5	49.81	118.9	1,88	3.08	64.49
	5x10⁻⁶	173.4	55.72	152.9	1.96	3.02	66.26
	7x10⁻⁶	136.2	53.92	140.5	1.92	2.81	73.5
	9x10⁻⁶	134.2	55.49	150.5	1.89	2.92	73.89
	11x10⁻⁶	109.1	52.83	127.9	1.95	3.1	78.77

	13x10⁻⁶	108.4	52.95	139.5	1.91	3.02	78.91
Compound (4)	5x10⁻⁶	479.1	62.15	93.77	1.91	2.79	6.78
	7x10⁻⁶	384	59.22	105	2.01	3.1	25.29
	9x10⁻⁶	378.1	49.43	63.68	1.99	3.01	26.43
	11x10⁻⁶	377.1	49.77	59	2.08	2.87	26.63
	13x10⁻⁶	357.5	46.08	51.08	1.79	3.04	30.44
	15x10⁻⁶	284.3	63.31	215.7	1.86	3	44.68

3.7. SEM investigation and EDX analysis

The formation of a protective surface film of inhibitor at the electrode surface was further confirmed by SEM observations of the metal surface. Also, in order to see whether the organic derivatives molecules are adsorbed on the copper surface or not, both SEM and EDX experiments were carried out. Figure (9) shows the scanning electron microscopy (SEM) micrograph of fresh copper surface without any additions of acid or the inhibitor. The morphological images for cupper surface exposed to 1 M HNO_3 solution without and with the addition of the optimum concentration of the organic derivatives are shown in Figure (9). As can be seen, there was a marked improvement in the surface morphology of copper that was treated with the inhibitor (the rate of corrosion is suppressed) due to the formation of an adsorbed protective film of the inhibitor at the sample surface.
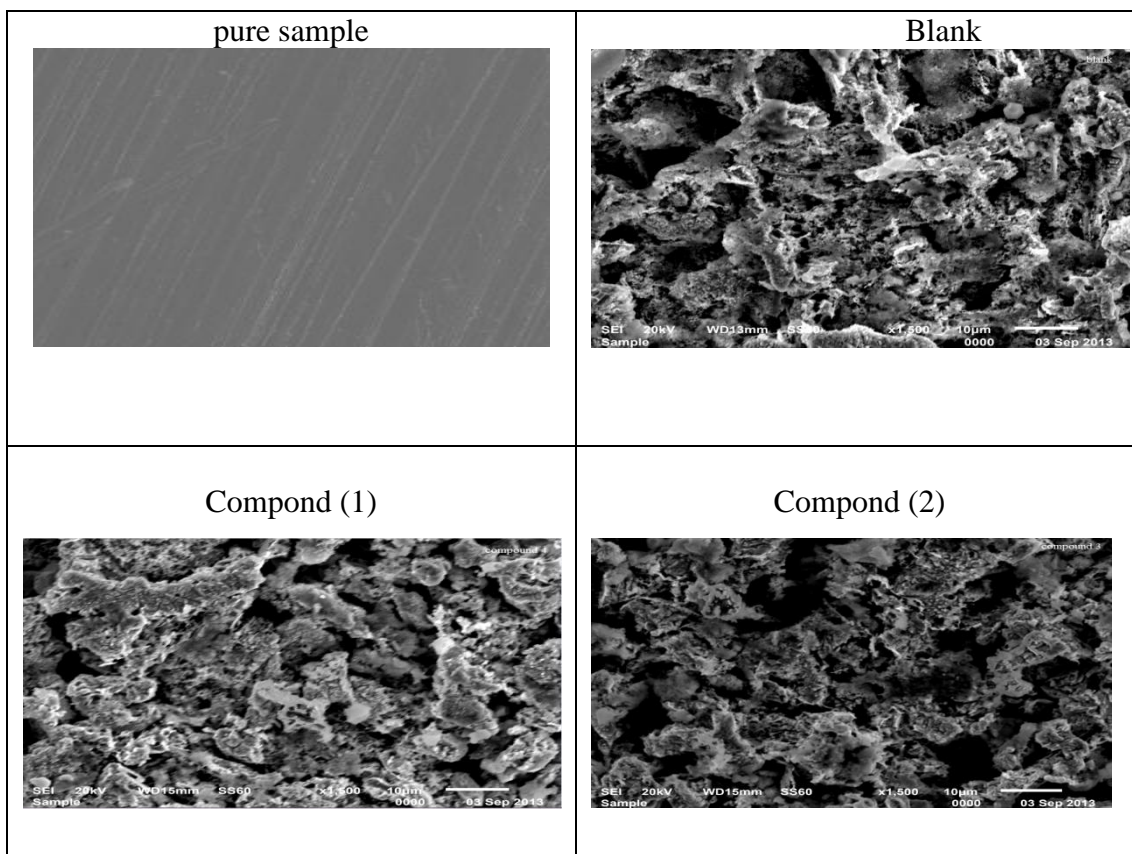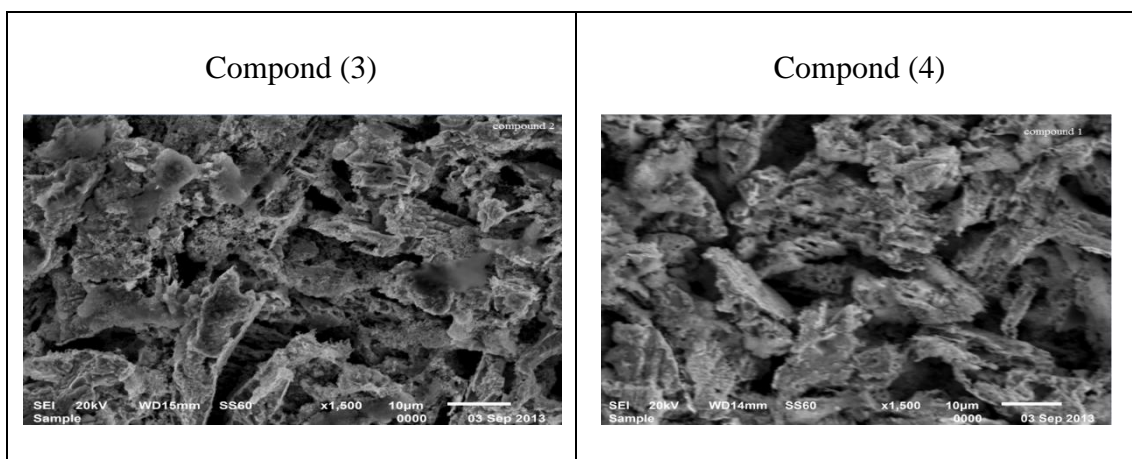
Figure 9. SEM micrographs for copper in absence and presence of 15×10^{-6} M of organic compounds

The corresponding Energy dispersive X-ray (EDX) profile analysis is presented in Figure (10). The EDX survey spectra were used to determine which elements of inhibitor were present on the electrode surface before and after exposure to the inhibitor solution. For the specimen without inhibitor treatment [Figure (10)] only copper was detected. This is confirmed by using XRD, the main corrosion products formed on exposed copper to nitric acid were identified as the basic copper nitrate, gerhardtite ($Cu_2(NO_3)(OH)_3$) and to a smaller extent cuprite (Cu_2O) [53, 54]. It is noticed the existence of the carbon, oxygen and nitrogen peak in the EDX spectra in the case of the sample exposed to the inhibitor, could be attributed to the adsorption of organic moiety at the copper surface. The increase in amount of carbon atom in the case of compound (1) (10.41 %) in comparison of compounds (4) (7.55%), indicated that the dissolution of copper is very inhibited by compound (1) and thereby shows a very high protective capacity, in contrast, the protective films formed by the compound (4) is very thin, especially in the case of compound (4). Also a strong enrichment with carbon is noted in the case of compound (1) (Table 9). The spectra of Figure (10) show that the oxygen signals are considerably suppressed relative to the samples prepared in 1M HNO_3 solution, and certainly this suppression will increase with increasing investigated concentrations and immersion time. The suppression of the oxygen signals takes place because of the overlying inhibitor film. Also it is important to notice the amount of copper peaks of EDX spectra is increased in the presence of inhibitor in a comparison of EDX analysis obtained in the absence of inhibitor may indicating that the investigated derivatives molecules protecting the copper surface against acid corrosion, in addition to the surface of the metal may not covered completely by the investigated molecules due to the short immersion time. The composition of the detected elements on the copper surface indicates that the inhibitor molecules are strongly adsorbed on the copper forming a Cu- investigated molecule bond, thus preventing the surface against corrosion.
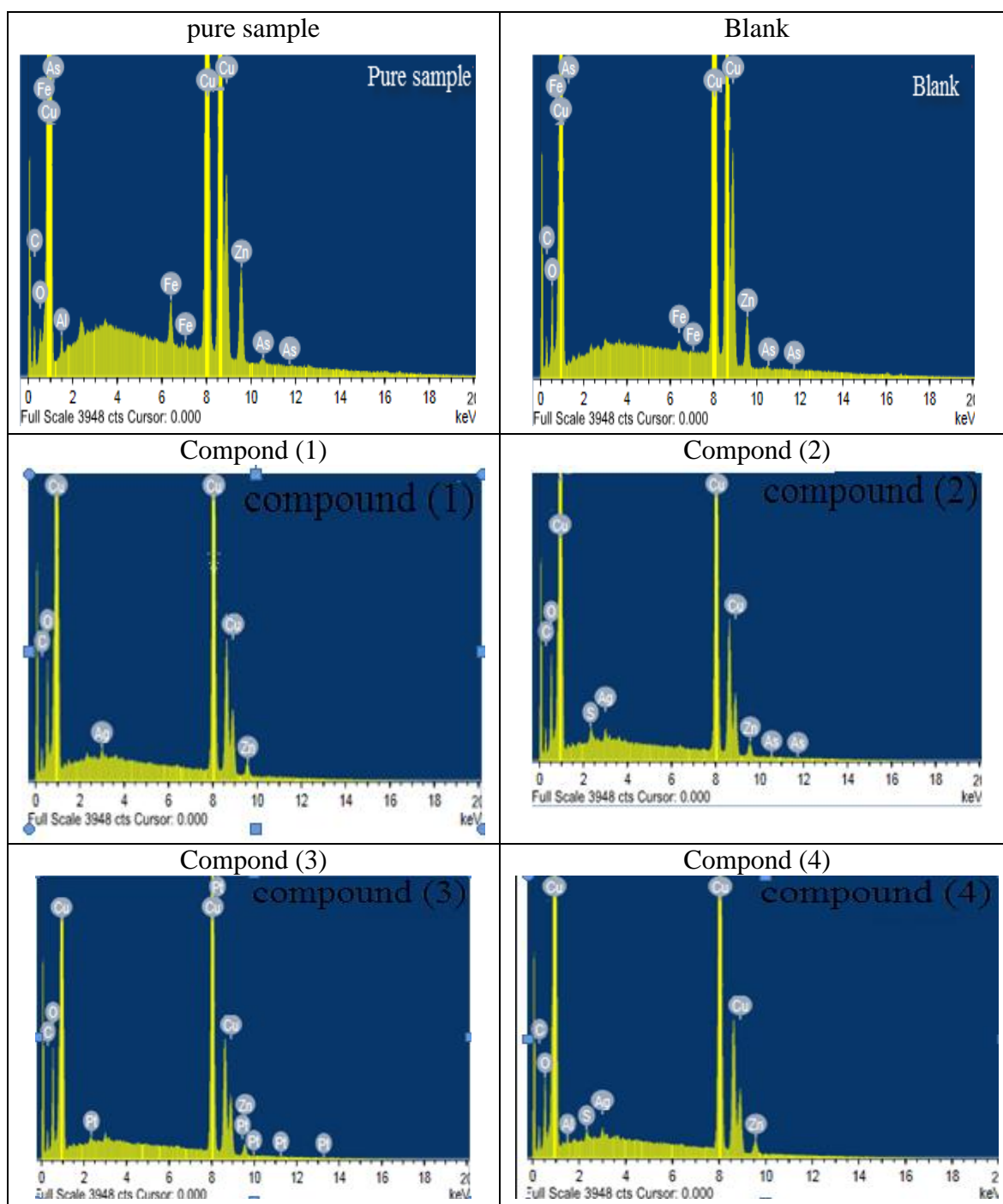
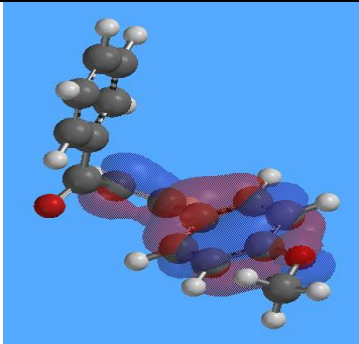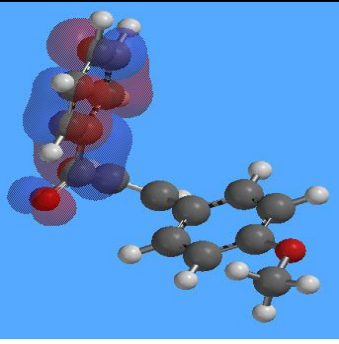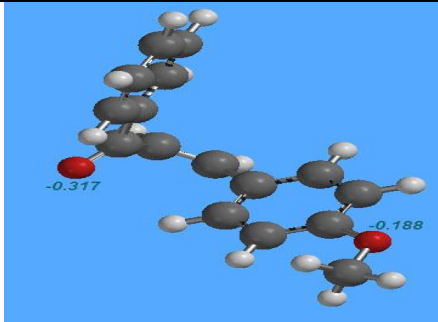**Figure 10.** EDX analysis for copper in absence and presence of 15 x10^{-6} M for 3 days immersion

Table 9. Surface composition (weight %) of copper after 3 days of immersion in HNO$_3$ without and with the optimum concentrations of the studied inhibitors

(Mass %)	Cu	Zn	C	O	As	Ag
Pure	80.78	2.72	12.48	2.13	0.40	----
Blank	60.45	1.74	7.42	15.85	0.25	----
Compound(1)	64.59	2.45	10.41	7.20	0.55	0.84

Compound(2)	64.45	2.78	8.43	6.80	0.25	0.74
Compound(3)	63.67	2.33	8.09	5.85	0.21	0.70
Compound(4)	62.57	2.17	7.55	4.86	----	----

3.8. Quantum chemical calculations

Figure 11 represents the molecular orbital plots and Mulliken charges of investigated compounds. Theoretical calculations were performed for only the neutral forms, in order to give further insight into the experimental results. Values of quantum chemical indices such as energies of lowest unoccupied molecular orbitals (LUMO) and energy of highest occupied molecular orbitals (HOMO) (E_{HOMO} and E_{LUMO}), the formation heat ΔH_f and energy gap ΔE, are calculated by semi-empirical AM1, MNDO and PM3 methods has been given in Table (10). It has been reported that the higher or less negative E_{HOMO} is associated of inhibitor, the greater the trend of offering electrons to unoccupied d orbital of the metal, and the higher the corrosion inhibition efficiency, in addition, the lower E_{LUMO}, the easier the acceptance of electrons from metal surface [54]. From Table (10), it is clear that ΔE obtained by the four methods in case of compound (4) is lower than compound (1), which enhance the assumption that compound (1) molecule will absorb more strongly on copper surface than compound (4), due to facilitating of electron transfer between molecular orbital HOMO and LUMO which takes place during its adsorption on the metal surface and thereafter presents the maximum of inhibition efficiency. Also it can be seen that E_{HOMO} increases from compound (1) to compound (4) facilitates the adsorption and the inhibition by supporting the transport process through the adsorbed layer. Reportedly, excellent corrosion inhibitors are usually those organic compounds who are not only offer electrons to unoccupied orbital of the metal, but also accept free electrons from the metal [55,56]. It can be seen that all calculated quantum chemical parameters validate these experimental results.

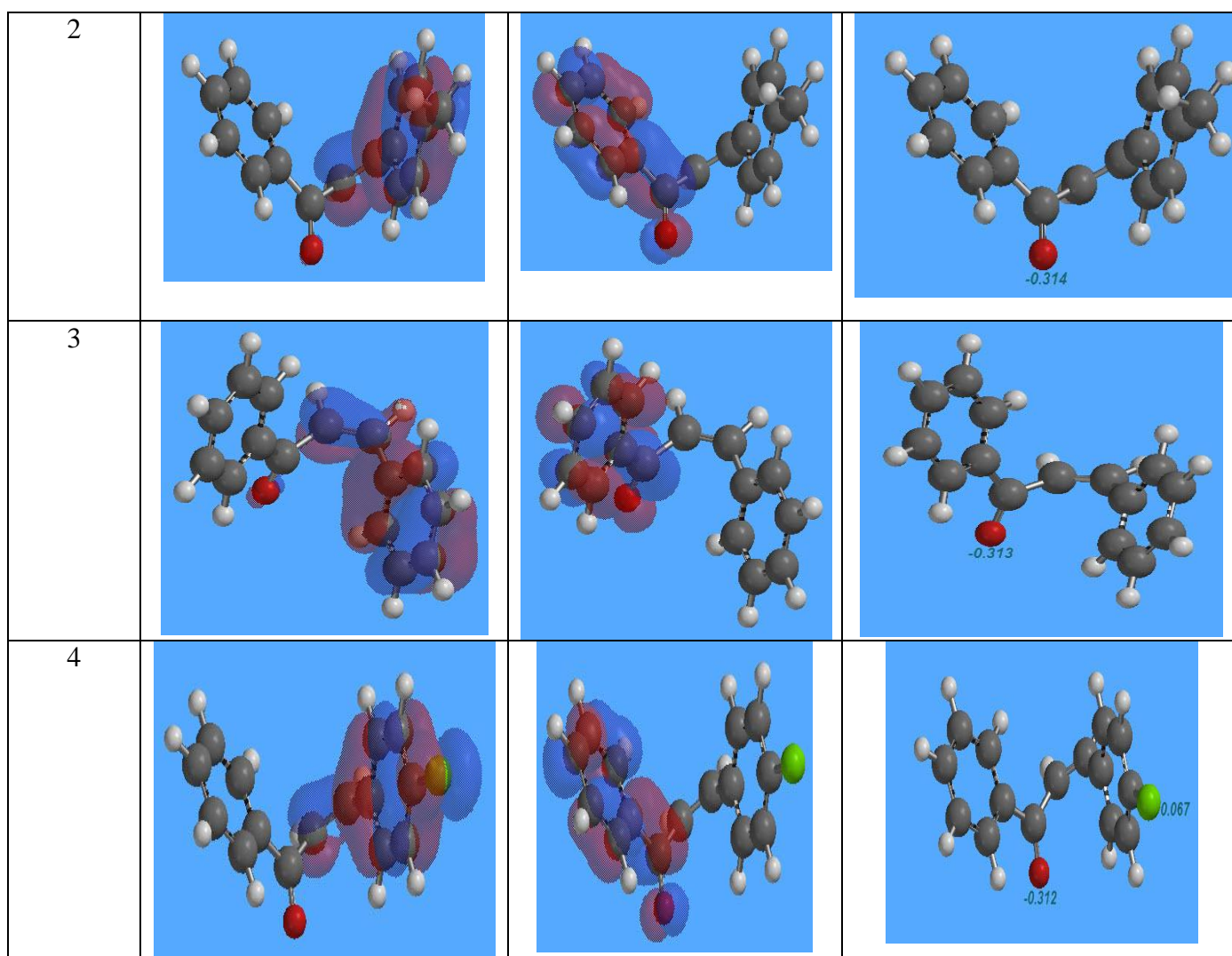| Structure	HOMO	LUMO	Mulliken charges
1			

Figure 11. Molecular orbital plots and Mulliken charges of organic compounds

Table 10. Calculated quantum chemical properties for organic compounds

	Compound (1)	Compound (2)	Compound (3)	Compound (4)
$-E_{HOMO}$ (eV)	9.01	9.28	9.29	9.54
$-E_{LUMO}$ (eV)	0.41	0.35	0.34	0.33
ΔE (eV)	8.600	8.920	8.940	9.210
η (eV)	4.300	4.460	4.470	4.605
σ (eV^{-1})	233	225	224	217
$-Pi$ (eV)	4.710	4.820	4.821	4.935
χ (eV)	4.710	4.820	4.821	4.935
Dipole moment,(Debye)	1.71	2.73	2.69	2.81
Area (Å^2)	280.71	270.62	251.13	266.08

3.9. Inhibition mechanism

Inhibition of the corrosion of copper in 1 M HNO_3 solution by investigated compounds is determined by weight loss, potentiodynamic polarization measurements, electrochemical impedance spectroscopy (EIS), electrochemical frequency modulation method (EFM) and Scanning Electron Microscopy (SEM) studies, it was found that the inhibition efficiency depends on concentration, nature of metal, the mode of adsorption of the inhibitors and surface conditions. The observed corrosion data in presence of these inhibitors, namely: i) The decrease of corrosion rate and corrosion current with increase in concentration of the inhibitor. ii) The linear variation of weight loss with time. iii) The shift in Tafel lines to higher potential regions. iv) The decrease in corrosion inhibition with increasing temperature indicates that desorption of the adsorbed inhibitor molecules takes place and v) the inhibition efficiency was shown to depend on the number of adsorption active centers in the molecule and their charge density. The corrosion inhibition is due to adsorption of the inhibitors at the electrode/ solution interface, the extent of adsorption of an inhibitor depends on the nature of the metal, the mode of adsorption of the inhibitor and the surface conditions. Adsorption on copper surface is assumed to take place mainly through the active centers attached to the inhibitor and would depend on their charge density. Transfer of lone pairs of electrons on the nitrogen atoms to the copper surface to form a coordinate type of linkage is favored by the presence of a vacant orbital in iron atom of low energy. Polar character of substituents in the changing part of the inhibitor molecule seems to have a prominent effect on the electron charge density of the molecule. It was concluded that the mode of adsorption depends on the affinity of the metal towards the π-electron clouds of the ring system. Metals such as Cu and Fe, which have a greater affinity towards aromatic moieties, were found to adsorb benzene rings in a flat orientation. The order of decreasing the percentage inhibition efficiency of the investigated inhibitors in the corrosive solution was as follow: compound (1) > compound (2) > compound (3) > compound (4).

Compound (1) exhibits excellent inhibition power due to: (i) the presence of   p-OCH_3 group which is an electron donating group with negative Hammett constant (σ = -0.27), Also this group will increase the electron charge density on the molecule and may be an additional active centre (ii) its larger molecular size that may facilitate better surface coverage, and (iii) its adsorption through two active centers a. Compound (2) comes after compound (1) in inhibition efficiency due to:(i) its lower molecular size than compound (1), and (ii) the presence of p-CH_3 with low Hammett constant than p-CH_3 (σ = - 0.17) which is lower electron releasing group than OCH_3group which enhance the delocalized π-electrons on the active centers of the compound. Compound (3) comes after compound (2) in inhibition efficiency because it has lower molecular size than compound (2) and has no substituent in p-position (H-atom with σ =0.0) which contributes no charge density to the molecule. Compound (4) has the lowest inhibition efficiency. This is due to presence of p- Cl which has positive Hammett constant (σ=+0.23).i.e. which lower the electron density on the molecule and hence, lower inhibition efficiency.

References

1. H.Y. Tsai, S.C. Sun, S.J. Wang, *J. Electrochem. Soc*. 147 (2000)2766.
2. A. Krishnamoorthy, K. Chanda, S.P. Murarka, G. Ramanath,J.G. Ryan, *Appl. Phys. Lett*. 78 (2001) 2467.
3. C.E. Ho, W.T. Chen, C.R. Kao, *J. Electron. Mater*. 30 (2001)379.
4. R.R. Thomas, V.A. Brusic, B.M. Rush, *J. Electrochem. Soc.* 139(1992) 678.
5. C. Fiaud, Proceedings of the Int. Symposium on Control of Copper and Copper Alloys Oxidation, Rouen, France, (1992).97.
6. D. Chadwick, T. Hashemi, *Corros. Sci*. 18 (1978) 39.
7. S.L.F.A. da Costa, S.M.L. Agostinho, *J. Electroanal. Chem*. 296(1990) 51.
8. H.A.A. El-Rahman, *Corrosion* 47 (1991) 424.
9. N. Bellakhal, K. Draou, A. Addou, J.L. Brisset, *J. Appl.Electrochem*. 30 (2000)595.
10. M.M. El-naggar, *J. Mater. Sci*. 35 (2000) 6189.
11. F. Zucchi, G. Trabanelli, C. Monticelli, *Corros. Sci*. 38 (1996)147.
12. D. Chadwick, T. Hashemi, *Surf. Sci.* 89 (1979) 649.
13. S. Yoshida, H. Ishida, *Appl. Surf. Sci.* 20 (1985) 497.
14. M.H. Wahdan, G.K. Gomma, *Mater. Chem. Phys*. 47 (1997) 176.
15. S.M. Song, C.E. Park, H.K. Yun, C.S. Hwang, S.Y. Oh, J.M.Park, *J. Adhesion Sci. Tehnol*. 12 (5) (1998) 541.
16. K. Hofmann, Imidazole and its Derivatives, Interscience Publishers,Inc, New York, 1953.
17. R. F.Anderson, S. S. Shinde, A.Maroz.*Org. Biomol. Chem*. 6(2008) 1973.
18. R. W. Bosch, J. Hubrecht, W. F. Bogaerts, B. C. Syrett, *Corrosion* 57 (2001) 60.
19. S. S. Abdel–Rehim, K. F. Khaled, N. S. Abd–Elshafi, *Electrochim. Acta* .51 (2006)6269.
20. A. N.Wiercinska, G.Dalmate, *Electrochim. Acta*.51(2006) 6179.
21. A.Yurt, A. Balaban, S.U Kandemir., G.Bereket, B.Erk, *Mater Chem. Phys*.85(2004) 420.
22. A.Y. Etre, *Appl. Surf. Sci*.252(2006) 8521.
23. W.J.Lorenz and F.Mansfeld, *Corros.Sci*. 21 (1981) 647.
24. G. Trabanelli, in "Corrosion Mechanisms" (Ed. F. Mansfeld) Marcel Dekker, New York, 119 (1987).
25. A. S. Fouda, A. Abd. E. Aal, A. B. Kandil, *J. Dasalination* 201 (2006) 216.
26. F.H. Asaf, M. Abou- Krisha, M. Khodari, F. EL-Cheihk, A. A. Hussien, *Mater Chem. Phys*., 93 (2002) 1.
27. A.Fiala, A. Chibani, A. Darchen, A. Boulkamh, K. Djebbar, Appl. Surf. Sci. 253(2007) 9347.
28. S.T. Arab and E.M. Noor, *Corrosion* 49 (1993) 122.
29. W. Durnie, R.D. Marco, A. Jefferson, B. Kinsella, *J. Electrochem. Soc*., 146 (1999) 1751.
30. J. M. Thomas and W. J. Thomas, Introduction to the Principles of Heterogeneous Catalysis, 5th Ed, Academic Press, London (1981) 14.
31. G. Quartarone, G. Moretti, T. Bellomi, G. Capobianco, A. Zingales, *Corrosion* 54 (1998) 606.
32. W.D. Bjorndahl, K. Nobe, *Corrosion* 40 (1984) 82.
33. Schumacher, A. Muller, W. Stockel, *J. Electroanal. Chem*. 219 (1987) 311.
34. W.H. Smyrl, in: J.O.M. Bockris, B.E. Conway, E. Yeager, R.E. White (Eds.), Comprehensive Treatise of Electrochemistry, Plenum Press, New York.4. (1981) 116.
35. G. Quartarone, T. Bellomi, A. Zingales, *Corros. Sci*. 45 (2003) 722.
36. J.W. Schltze, K. Wippermann, *Electrochim. Acta* 32 (1987) 823.
37. D.C. Silverman and J.E. Carrico, *National Association of Corrosion Engineers*, 44 (1988) 280.
38. W.J.Lorenz and F.Mansfeld, *Corros.Sci*. 21 (1981) 647.
39. D. D. Macdonald, M. C. Mckubre. "Impedance measurements in Electrochemical systems," Modern Aspects of Electrochemistry, J.O'M. Bockris, B.E. Conway, R.E.White, Eds., Plenum Press, New York, New York, .14(1962)81.
40. F. Mansfeld; *Corrosion*, 36(1981), 301.

41. C. Gabrielli, "Identification of Electrochemical processes by Frequency Response Analysis,"Solarton Instrumentation Group, 1980.
42. M. El Achouri, S. Kertit, H.M. Gouttaya, B. Nciri, Y. Bensouda, L. Perez, M.R.Infante, K. Elkacemi, *Prog. Org. Coat*., 43 (2001) 267.
43. J.R. Macdonald, W.B. Johanson, in: J.R. Macdonald (Ed.), Theory in Impedance Spectroscopy, John Wiley& Sons, New York, 1987.
44. S.F. Mertens, C. Xhoffer, B.C. Decooman, E. Temmerman, *Corrosion* 53 (1997) 381.
45. G. Trabanelli, C. Montecelli, V. Grassi, A. Frignani, *J. Cem. Concr., Res.* 35 (2005) 1804.
46. A. J. Trowsdate, B. Noble, S .J. Haris, I.S. R. Gibbins, G. E. Thomson, G. C. Wood,   *Corros. Sci.*, 38 (1996) 177.
47. F.m.Reis, H.G.de Melo and I.Costa, *J.Electrochem.Acta*, 51 (2006) 17.
48. M. Lagrenee, B. Mernari, M. Bouanis, M. Traisnel & F. Bentiss, *Corros. Sci.*, 44 (2002) 573.
49. E. McCafferty, N. Hackerman, *J. Electrochem. Soc.* 119 (1972) 146.
50. H. Ma, S. Chen, L. Niu. S. Zhao, S. Li, D. Li, J. *Appl. Electrochem* 32 (2002) 65.
51. E. Kus, F. Mansfeld, *Corros. Sci.* 48 (2006) 965.
52. G. A. Caigman, S. K. Metcalf, E. M. Holt, *J.Chem. Cryst*. 30 (2000) 415.
53. M. Vajpeyi, S. Gupta, Dhirendra and G. N. Pandey, *Corros. Prev. Control*, October (1985)102.
54. Samie, F., Tidblad, J., Kucera, V., Leygraf, C., 39, (2005) 7362.
55. Samie, F., Tidblad, J., Kucera, V., Leygraf, C., 40, (2006) 3631.
56. I. Lukovits, K. Palfi, E. Kalman, Corrosion, 53 (1997) 915. 74- P. Zhao, Q. Liang, Y. Li, *Appl. Surf. Sci*., 252 (2005) 1596.